



HAL
open science

Collapse of Critical Nematic Fluctuations in FeSe under Pressure

Pierre Massat, Yundi Quan, Romain Grasset, Marie-Aude Measson, Maximilien Cazayous, Alain Sacuto, Sandra Karlsson, Pierre Strobel, Pierre Toulemonde, Zhiping Yin, et al.

► **To cite this version:**

Pierre Massat, Yundi Quan, Romain Grasset, Marie-Aude Measson, Maximilien Cazayous, et al.. Collapse of Critical Nematic Fluctuations in FeSe under Pressure. *Physical Review Letters*, 2018, 121 (7), pp.077001. 10.1103/PhysRevLett.121.077001 . hal-01996212

HAL Id: hal-01996212

<https://hal.science/hal-01996212>

Submitted on 23 Mar 2022

HAL is a multi-disciplinary open access archive for the deposit and dissemination of scientific research documents, whether they are published or not. The documents may come from teaching and research institutions in France or abroad, or from public or private research centers.

L'archive ouverte pluridisciplinaire **HAL**, est destinée au dépôt et à la diffusion de documents scientifiques de niveau recherche, publiés ou non, émanant des établissements d'enseignement et de recherche français ou étrangers, des laboratoires publics ou privés.

Collapse of critical nematic fluctuations in FeSe under pressure

Pierre Massat,^{1,*} Yundi Quan,² Romain Grasset,¹ Marie-Aude Méasson,^{1,3} Maximilien Cazayous,¹ Alain Sacuto,¹ Sandra Karlsson,^{3,†} Pierre Strobel,³ Pierre Toulemonde,³ Zhiping Yin,^{2,‡} and Yann Gallais^{1,§}

¹*Laboratoire Matériaux et Phénomènes Quantiques,
UMR 7162 CNRS, Université Paris Diderot, Paris, France*

²*Department of Physics and Center for Advanced Quantum Studies,
Beijing Normal University, Beijing, 100875 China*

³*Université Grenoble Alpes, CNRS, Grenoble INP, Institut Néel, F-38000 Grenoble, France*

(Dated: May 30, 2018)

We report the evolution of the electronic nematic susceptibility in FeSe via Raman scattering as a function of hydrostatic pressure up to 5.8 GPa where the superconducting transition temperature T_c reaches its maximum. The critical nematic fluctuations observed at low pressure vanish above 1.6 GPa, indicating they play a marginal role in the four-fold enhancement of T_c at higher pressures. The collapse of nematic fluctuations appears to be linked to a suppression of low energy electronic excitations which manifests itself by optical phonon anomalies at around 2 GPa, in agreement with lattice dynamical and electronic structure calculations using local density approximation combined with dynamical mean field theory. Our results reveal two different regimes of nematicity in the phase diagram of FeSe under pressure: a d -wave Pomeranchuk instability of the Fermi surface at low pressure and a magnetic driven orthorhombic distortion at higher pressure.

The pairing mechanism of iron-based superconductors (Fe SC) is believed to result from interband spin fluctuations [1, 2]. The spin fluctuations scenario is motivated by the observation that the maximum superconducting transition temperature corresponds to the end point of a stripe-like magnetic phase in several Fe SC [3]. However the magnetic order is invariably preceded by, or concomitant with, an electron nematic phase whereby the electronic sub-system spontaneously breaks the four-fold tetragonal symmetry and induces an orthorhombic distortion of the lattice [4, 5]. In several Fe SC strong electron nematic fluctuations (NF) have been observed near the optimal critical temperature T_c [6–8], hinting that they could play a role too in the pairing mechanism. Recent theoretical works indeed support the idea that critical NF near a quantum critical point (QCP) are generically helpful for SC pairing [9–11]. However addressing the driving force behind electron nematicity and the role of critical NF in enhancing T_c remains a challenge in many Fe SC, as magnetic and nematic orderings often occur simultaneously.

In this context superconducting FeSe stands out for its unusual properties compared to other Fe SC [12]. In bulk form and at ambient pressure, it has relatively low T_c but displays a nematic phase without any sign of magnetic ordering, thus challenging magnetic driven scenarios of nematicity [13–17]. A strong increase of T_c is observed upon applying hydrostatic pressure, reaching ~ 37 K at ~ 6 GPa [18, 19]. While recent ARPES and transport measurements have suggested a possible link between the increases of T_c and changes in Fermi surface topology in FeSe [20–24], its pressure phase diagram also differs significantly from other prototypical Fe SC [25–30]. The nematic phase transition temperature T_S initially decreases with pressure, and merges at around 1.5 – 2 GPa with a pressure induced magnetic

phase which is likely similar to the stripe-ordered phase observed in other Fe SC [28, 31–33]. The temperature $T_{S,m}$ of the resulting coupled magneto-structural transition has a non-monotonic pressure dependence terminating close to optimal pressure where T_c is maximum [27] (figure 1(a)), suggesting the presence of a QCP and questioning the respective roles of critical magnetic and nematic fluctuations in the pressure-induced four-fold enhancement of T_c .

In this letter we report the temperature and pressure dependence of the NF in bulk FeSe single crystals using Raman spectroscopy up to 5.8 GPa. We show that temperature dependent critical NF disappear rapidly upon increasing pressure and essentially vanish above 1.6 GPa, indicating two different regimes of nematicity: a low pressure regime where the nematic transition is driven by a d -wave Pomeranchuk instability of the Fermi surface, and a higher pressure regime where it is only a secondary symmetry breaking induced by the magnetic transition, implying that the enhancement of T_c above 2 GPa is not driven by critical NF in this pressure range. We further show that the disappearance of the critical NF is accompanied by anomalies in the pressure dependence of Raman-active optical phonons' frequencies. Supported by density functional theory plus dynamical mean-field theory calculations, we link the phonon anomalies and the collapse of NF at ~ 2 GPa to a Lifshitz transition of the Fermi surface.

Raman measurements under pressure were performed using a membrane diamond anvil cell (DAC) allowing continuous change of pressure at low temperature, and designed with a large numerical aperture as described in [34, 35]. Helium was used as the pressure transmitting medium. Figure 1(b) shows a sketch of the pressure cell and a photograph of the sample inside the cell. Focus was made on Raman spectra taken in the B_{1g} symmetry

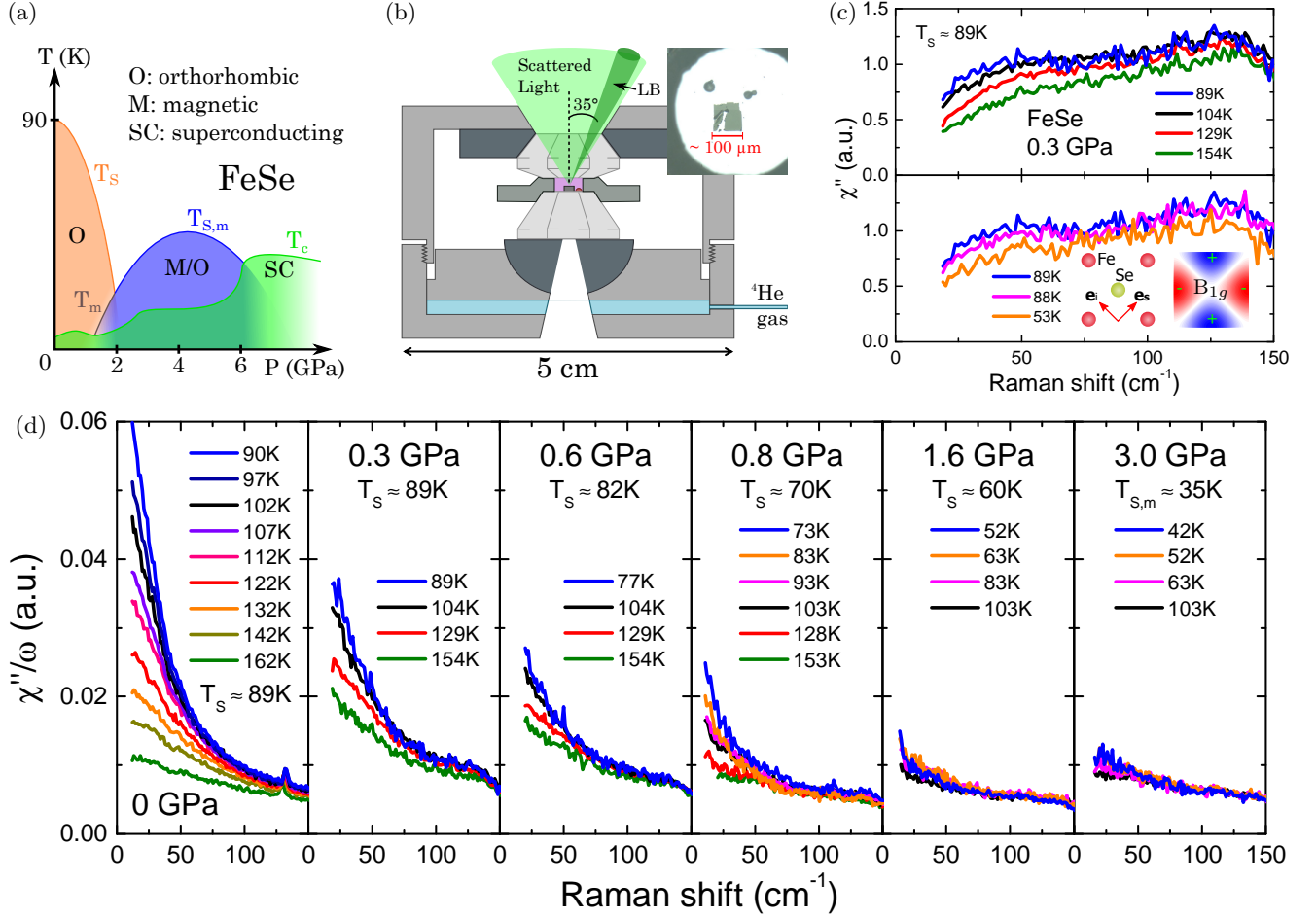


Figure 1. Raman spectroscopy of FeSe under hydrostatic pressure. (a) Schematic phase diagram of FeSe under pressure. (b) Side view sketch of the Raman pressure cell. LB stands for Laser Beam. Inset shows a top view photograph of the sample inside the pressure cell, with three ruby balls above it. (c) Temperature dependence above (upper panel) and below T_S (lower panel) of the B_{1g} Raman response at 0.3 GPa. Insets show the $x'y'$ polarizations configuration and the amplitude of the corresponding B_{1g} Raman vertex in momentum space. (d) Temperature dependent Raman conductivity $\chi''(\omega)/\omega$ measured at $P = 0, 0.3, 0.6, 0.8, 1.6$ and 3.0 GPa. The data at 0.3 GPa are the same as that of (c) (divided by frequency).

[36] which, in the 1-Fe unit cell notation, corresponds to the nematic order observed in FeSe at ambient pressure [37].

Figure 1(c) displays the temperature dependence of the Raman response in B_{1g} symmetry at 0.3 GPa. It follows the behavior of the Raman spectra of FeSe at ambient pressure reported earlier [37]. When approaching the nematic transition from high temperatures, the growth of critical NF manifests itself by an increase in the low energy Raman response $\chi''(\omega)$ upon approaching T_S , and a subsequent decrease in the nematic phase below T_S .

The temperature dependence of the B_{1g} Raman conductivity χ''/ω , which controls the static nematic susceptibility (see equation 1 below), is plotted at different pressures in figure 1(d). For clarity only spectra above the estimated T_S , which is 89K at 0 GPa but decreases when increasing pressure [26, 38], are shown. The spectra at 0 GPa were taken outside the pressure

cell on a different crystal from the same batch, and are shown here for comparison. In the Raman conductivity spectrum the NF appear as a quasi-elastic peak (QEP) centered at zero-energy [39]. At low pressures, below 0.8 GPa, the QEP intensity increases significantly when lowering temperature down to T_S , following the behavior observed at ambient pressure. However upon increasing pressure the maximum intensity of the QEP close to T_S (blue curve at each pressure), and its overall enhancement decrease significantly. At 1.6 GPa and 3.0 GPa the QEP is barely visible and shows negligible enhancement upon cooling.

In order to quantify the observed pressure evolution of NF, we computed the static B_{1g} nematic susceptibility $\chi_0^{B_{1g}}$, obtained from the Raman conductivity through the Kramers-Kronig relation:

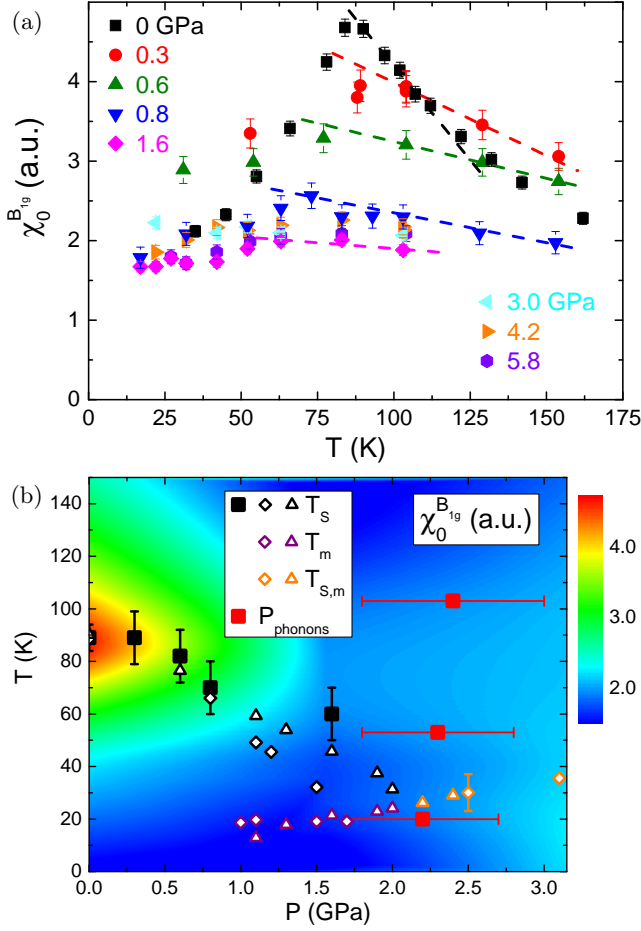


Figure 2. (a) Temperature dependence of the static nematic susceptibility $\chi_0^{B_{1g}}$ at different pressures between 0 and 5.8 GPa. Dashed lines are linear fits showing the slope at 100 K: $\left. \frac{d\chi_0^{B_{1g}}}{dT} \right|_{100 \text{ K}}$ at each pressure from 0 to 1.6 GPa; within experimental accuracy, the slope is 0 above 3 GPa. (b) Color map of the static nematic susceptibility $\chi_0^{B_{1g}}$ as a function of temperature and pressure, plotted using the data points in (a). The color scale is in arbitrary units. The temperatures of the structural (T_S), magnetic (T_m) and magneto-structural ($T_{S,m}$) transitions are indicated by black, purple and orange symbols respectively. Full squares: this work; empty diamonds: [28]; empty triangles: [31]. Red squares with error bars indicate the pressure range of the phonon anomalies at 103 K, 53 K and 20 K (see text).

$$\chi_0(T, P) = \int_0^\infty \frac{\chi''(\omega, T, P)}{\omega} d\omega \quad (1)$$

The integral was performed over the whole frequency range accessible from our data, i.e. from 0 to 470 cm^{-1} , with the data at low energy resulting from linear extrapolation of the Raman response between 0 and 12 cm^{-1} . The resulting temperature dependence of the nematic susceptibility at each pressure is plotted in figure 2(a) where we have included additional points at higher pres-

ures: 4.2 GPa and 5.8 GPa. At low pressures $\chi_0^{B_{1g}}$ increases when lowering temperature, reaches a maximum at $T_S(P)$ and decreases inside the nematic phase. The pressure evolution of $\chi_0^{B_{1g}}(T)$ indicates a change of regime of NF upon increasing pressure: while the increase of $\chi_0^{B_{1g}}$ when lowering temperature down to T_S is still significant at 0.8 GPa, indicating sizable critical NF close to T_S at this pressure, it is much weaker at 1.6 GPa and there is essentially no increase at 3 GPa and above. Besides, at 4.2 GPa and 5.8 GPa the static susceptibility shows a small but clear suppression below $\sim 40 \text{ K}$ and $\sim 60 \text{ K}$ respectively, which might be linked to the magneto-orthorhombic transition.

The evolution of $\chi_0^{B_{1g}}$ with temperature and pressure is summarized in a colormap phase diagram in figure 2(b). Also plotted are the values of the structural (T_S), magnetic (T_m) and magneto-structural ($T_{S,m}$) transitions as reported in [28, 31], along with the structural transition temperatures extracted from our data as the temperature at which $\chi_0^{B_{1g}}$ is maximum. The latter are consistent with those of [28, 31], except at 1.6 GPa where our value appears somewhat higher.

The collapse of critical NF in the charge channel while magnetism emerges upon increasing pressure indicates that the nematic transition is not magnetic-driven at low pressures, below $\sim 1.6 \text{ GPa}$, but is rather driven by a d -wave Pomeranchuk instability of the Fermi surface, whose associated charge NF contribute to Raman scattering [39–41]. By contrast, at higher pressures, the absence of critical NF can naturally be linked to a fast weakening of this instability, and strongly suggests that the orthorhombic distortion in this regime is only a mere consequence of stripe-like magnetic ordering. The pressure induced change in the driving force of nematicity naturally explains the absence of scaling between the orthorhombic distortion and the ordered magnetic moment reported recently by X-ray and Mössbauer measurements in FeSe under pressure [30].

Our findings also imply a marginal role of critical NF in the enhancement of T_c observed between 2 and 6 GPa, and their absence at 5.8 GPa near the putative QCP contrasts with the divergent nematic susceptibility observed near $T_{c,\text{max}}$ in several Fe SC [6–8, 42]. Therefore, while we cannot rule out a role of NF in the pairing mechanism, the strong enhancement of T_c in FeSe under pressure cannot be associated to the presence of a nematic QCP [10, 11]. It is noteworthy that the disappearance of critical NF coincides with the merging of the magnetic and structural transitions into a coupled first-order transition, which occurs between 1.5 GPa and 2.0 GPa (see figure 2b) [28, 31]. As we show below, the evolution of optical phonons under pressure points to a change in the low energy band structure in the same pressure range, providing an underlying cause for these phenomena.

In figure 3 we plot the pressure evolutions of the fre-

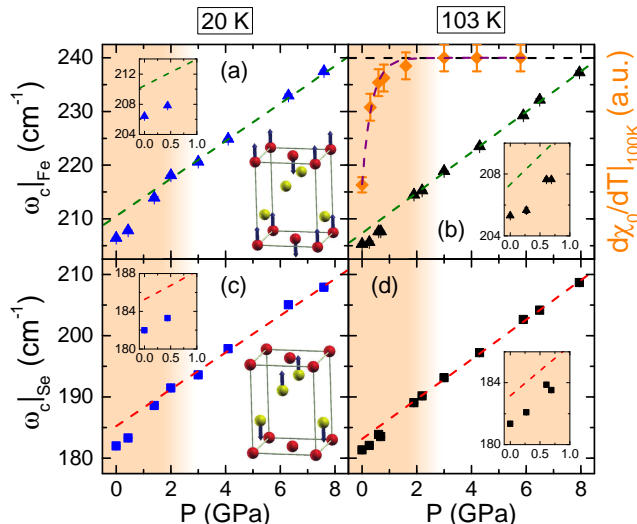


Figure 3. Pressure dependences of both Fe (B_{2g} , triangles, top row) and Se (A_{1g} , squares, bottom row) phonons' energies at 20 K (left column, blue) and 103 K (right column, black). Dashed lines are linear fits of the data points for $P > 2$ GPa. Motions of the atoms are shown as insets in (a) and (c): Fe and Se atoms are in red and yellow respectively (reproduced from [43]). An anomalous softening of 1–2% at 0 GPa is clear from the low pressure zooms shown as insets. Also plotted in (b) with orange diamonds is the pressure dependence of the slope of the static susceptibility $\left. \frac{d\chi_0^{B_{1g}}}{dT} \right|_{100\text{K}}$ as extracted from the linear fits in figure 2(a); the purple dashed line is a guide to the eye; the horizontal black dashed line indicates $d\chi_0/dT = 0$.

quencies of two Raman active phonons at 103 K and 20 K. The A_{1g} (resp. B_{2g}) symmetry phonon involves the motion of the Selenium (resp. Iron) atoms out of plane. Between 2 GPa and 8 GPa the phonon frequencies display a linear pressure hardening consistent with lattice contraction. However below 2 ± 0.5 GPa a clear frequency softening, which manifests itself by a deviation from linearity in the pressure dependence, is observed for both phonons. For the B_{2g} Fe phonon a linewidth broadening is also observed [36]. Importantly, while the observed deviations are stronger at 20 K, they are also visible at 53 K [36] and 103 K, implying that they are not mere consequences of the magnetostructural transition nor of the superconducting transition, which respectively occur below 60 K and 40 K at all pressures [25, 27, 28, 38]. We note that anomalies of the structural parameters have been reported in the same pressure range at low temperature [29, 44].

In order to clarify the origin of the phonon anomalies, we performed theoretical calculations of the band structure and the phonon energies under pressure, using local density approximation combined with dynamical mean-field theory (LDA+DMFT, figure 4a, b) [45] in the paramagnetic state (PM). Remarkably the calculations display a clear softening of both phonons' frequen-

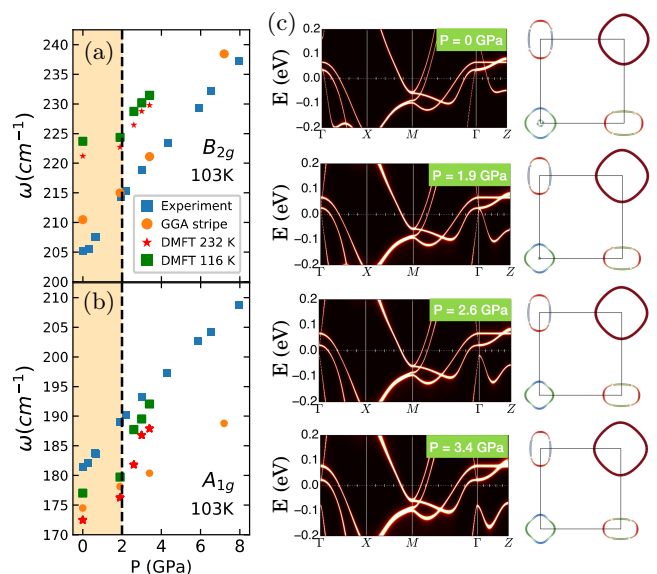


Figure 4. LDA+DMFT calculations of FeSe phonons and band structure under pressure. (a) B_{2g} and (b) A_{1g} phonon frequencies at $\mathbf{q} = 0$. Blue squares: experimental data at 103 K (see figures 3). Green squares and red stars: phonon frequencies obtained from LDA+DMFT calculations in the PM state at 116 K and 232 K respectively. Orange circles: phonon frequencies from DFT-GGA calculations in the stripe AFM state. (c) Band structure (left column) and orbitally-resolved 2D Fermi surface (right column) of FeSe calculated by LDA+DMFT at 0 GPa, 1.9 GPa, 2.6 GPa and 3.4 GPa. Red, green and blue colors denote dominating d_{xy} , d_{xz} and d_{yz} orbital characters, respectively.

cies at ~ 2 GPa. In this pressure range, the calculated electronic structure undergoes a Lifshitz transition due to the disappearance of the inner hole pocket at the Γ point between 1.9 GPa and 2.6 GPa (fig. 4(c), see also [46]), suggesting the phonon anomalies are associated to a change in Fermi surface topology [47]. On the other hand, the phonon frequencies calculated using DFT in the general gradient approximation (GGA) in the stripe magnetic phase, where no Lifshitz transition occurs, do not show any significant anomaly in the whole pressure range investigated (figure 4). In this scenario the phonon softening below 2 GPa is associated to the emergence of additional low energy electronic excitations to which the optical phonons couple [48, 49].

The link between Fermi surface topology and the strength of critical NF appears clearly when plotting together the evolution under pressure of the Fe phonon frequency and that of the slope of the nematic susceptibility, both at 103 K (figure 3b): the latter goes to zero in the same pressure interval where the former recovers linearity. This suggests that the low energy electronic states responsible for the phonon softening at low pressure also drive strong critical NF, causing a change in the regime of nematicity below ~ 2 GPa. Our findings are consistent with several theoretical studies which

have shown that the strength of the nematic and magnetic couplings strongly depend on the size, the orbital content and the nesting conditions of the hole and electron pockets [40, 50–55].

To conclude it is interesting to contrast the evolution of critical NF in FeSe under pressure with the case of 122 Fe SC. Recent works have highlighted strong similarities between the pressure phase diagram of FeSe and the doping phase diagram of BaFe_2As_2 [28, 30]. However we note that critical NF are observed in both hole and electron doped BaFe_2As_2 close to their optimal T_c [8, 56, 57]. In addition, magnetic and nematic fluctuations are strongly linked in BaFe_2As_2 [58] while they appear to be essentially decoupled in FeSe. This suggests that while the phase diagrams of both systems may appear similar from the point of view of the ordered phases, they are fundamentally different in the nature of the dominant fluctuations and their interplay.

P.M. and Y.G. are grateful to Lara Benfatto, Rafael Fernandes, Laura Fanfarillo, Peter Hirschfeld, Alaska Subedi and Belen Valenzuela for useful discussions. Y. G. also acknowledges Indranil Paul for numerous insightful comments and discussions. P.T. acknowledges the financial support of UGA and Grenoble INP through the AGIR-2013 contract of S. Karlsson. Z.P.Y. and Y.Q. were supported by the National Natural Science Foundation of China (Grant No. 11674030, 11704034), the Fundamental Research Funds for the Central Universities (Grant No. 310421113) and the National Key Research and Development Program of China through Contract No. 2016YFA0302300. The calculations used high performance clusters at the National Supercomputer Center in Guangzhou.

The authors declare no competing interests.

* pierre.massat@paris7.jussieu.fr

† Present address: Department of Quantum Matter, Physics University of Geneva, 24 Quai Ernest-Ansermet - 1211 Geneva 4

‡ yinzhiping@bnu.edu.cn

§ yann.gallais@paris7.jussieu.fr

- [1] K. Kuroki, S. Onari, R. Arita, H. Usui, Y. Tanaka, H. Kontani, and H. Aoki, *Phys. Rev. Lett.* **101**, 087004 (2008).
- [2] I. I. Mazin, D. J. Singh, M. D. Johannes, and M. H. Du, *Physical Review Letters* **101**, 057003 (2008).
- [3] D. C. Johnston, *Advances in Physics* **59**, 803 (2010).
- [4] J.-H. Chu, J. G. Analytis, K. De Greve, P. L. McMahon, Z. Islam, Y. Yamamoto, and I. R. Fisher, *Science* **329**, 824 (2010).
- [5] R. M. Fernandes, A. V. Chubukov, and J. Schmalian, *Nat Phys* **10**, 97 (2014).
- [6] J.-H. Chu, H.-H. Kuo, J. G. Analytis, and I. R. Fisher, *Science* **337**, 710 (2012).
- [7] Y. Gallais, R. M. Fernandes, I. Paul, L. Chauvière, Y.-X. Yang, M.-A. Méasson, M. Cazayous, A. Sacuto, D. Colson, and A. Forget, *Phys. Rev. Lett.* **111**, 267001 (2013).
- [8] H.-H. Kuo, J.-H. Chu, J. C. Palmstrom, S. A. Kivelson, and I. R. Fisher, *Science* **352**, 958 (2016).
- [9] T. A. Maier and D. J. Scalapino, *Phys. Rev. B* **90**, 174510 (2014).
- [10] S. Lederer, Y. Schattner, E. Berg, and S. A. Kivelson, *Phys. Rev. Lett.* **114**, 097001 (2015).
- [11] D. Labat and I. Paul, *Phys. Rev. B* **96**, 195146 (2017).
- [12] A. I. Coldea and M. D. Watson, *Annual Review of Condensed Matter Physics* **9**, 125 (2018).
- [13] F.-C. Hsu, J.-Y. Luo, K.-W. Yeh, T.-K. Chen, T.-W. Huang, P. M. Wu, Y.-C. Lee, Y.-L. Huang, Y.-Y. Chu, D.-C. Yan, and M.-K. Wu, *Proceedings of the National Academy of Sciences* **105**, 14262 (2008).
- [14] T. M. McQueen, A. J. Williams, P. W. Stephens, J. Tao, Y. Zhu, V. Ksenofontov, F. Casper, C. Felser, and R. J. Cava, *Phys. Rev. Lett.* **103**, 057002 (2009).
- [15] S.-H. Baek, D. V. Efremov, J. M. Ok, J. S. Kim, J. van den Brink, and B. Büchner, *Nature Materials* **14**, 210 (2014).
- [16] A. E. Böhrer, T. Arai, F. Hardy, T. Hattori, T. Iye, T. Wolf, H. v. Löhneysen, K. Ishida, and C. Meingast, *Phys. Rev. Lett.* **114**, 027001 (2015).
- [17] M. D. Watson, T. K. Kim, A. A. Haghighirad, N. R. Davies, A. McCollam, A. Narayanan, S. F. Blake, Y. L. Chen, S. Ghannadzadeh, A. J. Schofield, M. Hoesch, C. Meingast, T. Wolf, and A. I. Coldea, *Phys. Rev. B* **91**, 155106 (2015).
- [18] S. Medvedev, T. M. McQueen, I. A. Troyan, T. Palasyuk, M. I. Eremets, R. J. Cava, S. Naghavi, F. Casper, V. Ksenofontov, G. Wortmann, and C. Felser, *Nat Mater* **8**, 630 (2009).
- [19] G. Garbarino, A. Sow, P. Lejay, A. Sulpice, P. Toulemonde, M. Mezouar, and M. Núñez-Regueiro, *EPL (Europhysics Letters)* **86**, 27001 (2009).
- [20] Z. R. Ye, C. F. Zhang, H. L. Ning, W. Li, L. Chen, T. Jia, M. Hashimoto, D. H. Lu, Z.-X. Shen, and Y. Zhang, *ArXiv* **1512.02526** (2015).
- [21] Y. Miyata, K. Nakayama, K. Sugawara, T. Sato, and T. Takahashi, *Nat Mater* **14**, 775 (2015).
- [22] B. Lei, J. H. Cui, Z. J. Xiang, C. Shang, N. Z. Wang, G. J. Ye, X. G. Luo, T. Wu, Z. Sun, and X. H. Chen, *Phys. Rev. Lett.* **116**, 077002 (2016).
- [23] J. Shiogai, T. Miyakawa, Y. Ito, T. Nojima, and A. Tsukazaki, *Phys. Rev. B* **95**, 115101 (2017).
- [24] J. P. Sun, G. Z. Ye, P. Shahi, J.-Q. Yan, K. Matsuura, H. Kontani, G. M. Zhang, Q. Zhou, B. C. Sales, T. Shibauchi, Y. Uwatoko, D. J. Singh, and J.-G. Cheng, *Phys. Rev. Lett.* **118**, 147004 (2017).
- [25] M. Bendele, A. Ichsanow, Y. Pashkevich, L. Keller, T. Strässle, A. Gusev, E. Pomjakushina, K. Conder, R. Khasanov, and H. Keller, *Phys. Rev. B* **85**, 064517 (2012).
- [26] T. Terashima, N. Kikugawa, S. Kasahara, T. Watashige, T. Shibauchi, Y. Matsuda, T. Wolf, A. E. Böhrer, F. Hardy, C. Meingast, H. v. Löhneysen, and S. Uji, *Journal of the Physical Society of Japan*, *J. Phys. Soc. Jpn.* **84**, 063701 (2015).
- [27] J. P. Sun, K. Matsuura, G. Z. Ye, Y. Mizukami, M. Shimozawa, K. Matsubayashi, M. Yamashita, T. Watashige, S. Kasahara, Y. Matsuda, J. Q. Yan, B. C. Sales, Y. Uwatoko, J. G. Cheng, and T. Shibauchi, *Nat. Comm.* **7**, (2016).

- [28] K. Kothapalli, A. E. Böhmer, W. T. Jayasekara, B. G. Ueland, P. Das, A. Sapkota, V. Taufour, Y. Xiao, E. Alp, S. L. Bud'ko, P. C. Canfield, A. Kreyssig, and A. I. Goldman, *Nat. Comm.* **7**, 12728 (2016).
- [29] V. Svitlyk, M. Raba, V. Dmitriev, P. Rodière, P. Toulemonde, D. Chernyshov, and M. Mezouar, *Phys. Rev. B* **96**, 014520 (2017).
- [30] A. E. Böhmer, K. Kothapalli, W. T. Jayasekara, J. M. Wilde, B. Li, A. Sapkota, B. G. Ueland, P. Das, Y. Xiao, W. Bi, J. Zhao, E. Ercan Alp, S. L. Bud'ko, P. C. Canfield, A. I. Goldman, and A. Kreyssig, *ArXiv e-prints* **1803.09449** (2018).
- [31] P. S. Wang, S. S. Sun, Y. Cui, W. H. Song, T. R. Li, R. Yu, H. Lei, and W. Yu, *Phys. Rev. Lett.* **117**, 237001 (2016).
- [32] A. E. Böhmer and A. Kreisel, *Journal of Physics: Condensed Matter* **30**, 023001 (2018).
- [33] R. Khasanov, R. M. Fernandes, G. Simutis, Z. Guguchia, A. Amato, H. Luetkens, E. Morenzoni, X. Dong, F. Zhou, and Z. Zhao, *ArXiv e-prints* **1804.04169** (2018).
- [34] J. Buhot, C. Toulouse, Y. Gallais, A. Sacuto, R. de Sousa, D. Wang, L. Bellaiche, M. Bibes, A. Barthélémy, A. Forget, D. Colson, M. Cazayous, and M.-A. Measson, *Phys. Rev. Lett.* **115**, 267204 (2015).
- [35] R. Grasset, T. Cea, Y. Gallais, M. Cazayous, A. Sacuto, L. Cario, L. Benfatto, and M.-A. Méasson, *Phys. Rev. B* **97**, 094502 (2018).
- [36] See Supplementary Material where references [59–80] are cited and for more detailed experimental and theoretical results and analysis.
- [37] P. Massat, D. Farina, I. Paul, S. Karlsson, P. Strobel, P. Toulemonde, M.-A. Méasson, M. Cazayous, A. Sacuto, S. Kasahara, T. Shibauchi, Y. Matsuda, and Y. Gallais, *Proceedings of the National Academy of Sciences* **113**, 9177 (2016).
- [38] K. Miyoshi, K. Morishita, E. Mutou, M. Kondo, O. Seida, K. Fujiwara, J. Takeuchi, and S. Nishigori, *Journal of the Physical Society of Japan*, *J. Phys. Soc. Jpn.* **83**, 013702 (2014).
- [39] Y. Gallais and I. Paul, *Comptes Rendus Physique* **17**, 113 (2016).
- [40] Y. Yamakawa, S. Onari, and H. Kontani, *Phys. Rev. X* **6**, 021032 (2016).
- [41] A. V. Chubukov, M. Khodas, and R. M. Fernandes, *Phys. Rev. X* **6**, 041045 (2016).
- [42] S. Hosoi, K. Matsuura, K. Ishida, H. Wang, Y. Mizukami, T. Watashige, S. Kasahara, Y. Matsuda, and T. Shibauchi, *Proceedings of the National Academy of Sciences* **113**, 8139 (2016).
- [43] Q.-Q. Ye, K. Liu, and Z.-Y. Lu, *Phys. Rev. B* **88**, 205130 (2013).
- [44] S. Margadonna, Y. Takabayashi, Y. Ohishi, Y. Mizuguchi, Y. Takano, T. Kagayama, T. Nakagawa, M. Takata, and K. Prassides, *Phys. Rev. B* **80**, 064506 (2009).
- [45] G. Kotliar, S. Y. Savrasov, K. Haule, V. S. Oudovenko, O. Parcollet, and C. A. Marianetti, *Rev. Mod. Phys.* **78**, 865 (2006).
- [46] S. Mandal, R. E. Cohen, and K. Haule, *Phys. Rev. B* **89**, 220502 (2014).
- [47] I. M. Lifshitz, *Soviet Physics JEPT* **11**, 1130 (1960).
- [48] F. Cerdeira and M. Cardona, *Phys. Rev. B* **5**, 1440 (1972).
- [49] E. Maksimov and S. Shulga, *Solid State Communications* **97**, 553 (1996).
- [50] R. M. Fernandes, A. V. Chubukov, J. Knolle, I. Eremin, and J. Schmalian, *Phys. Rev. B* **85**, 024534 (2012).
- [51] I. Paul, *Phys. Rev. B* **90**, 115102 (2014).
- [52] A. V. Chubukov and R.-Q. Xing, *Phys. Rev. B* **93**, 165141 (2016).
- [53] L. Fanfarillo, L. Benfatto, and B. Valenzuela, *Phys. Rev. B* **97**, 121109 (2018).
- [54] L. Classen, R.-Q. Xing, M. Khodas, and A. V. Chubukov, *Phys. Rev. Lett.* **118**, 037001 (2017).
- [55] J. Ishizuka, T. Yamada, Y. Yanagi, and Y. Ono, *Journal of the Physical Society of Japan* **87**, 014705 (2018).
- [56] A. E. Böhmer, P. Burger, F. Hardy, T. Wolf, P. Schweiss, R. Fromknecht, M. Reinecker, W. Schranz, and C. Meingast, *Phys. Rev. Lett.* **112**, 047001 (2014).
- [57] T. Böhm, R. Hosseinian Ahangharnejhad, D. Jost, A. Baum, B. Muschler, F. Kretzschmar, P. Adelman, T. Wolf, H. Wen, J. Chu, I. R. Fisher, and R. Hackl, *Physica Status Solidi (B)* **254**, 1600308 (2017).
- [58] R. M. Fernandes, A. E. Böhmer, C. Meingast, and J. Schmalian, *Phys. Rev. Lett.* **111**, 137001 (2013).
- [59] A. E. Böhmer, F. Hardy, F. Eilers, D. Ernst, P. Adelman, P. Schweiss, T. Wolf, and C. Meingast, *Phys. Rev. B* **87**, 180505 (2013).
- [60] S. Karlsson, P. Strobel, A. Sulpice, C. Marcenat, M. Legendre, F. Gay, S. Pairis, O. Leynaud, and P. Toulemonde, *Superconductor Science and Technology* **28**, 105009 (2015).
- [61] V. Gnezdilov, Y. G. Pashkevich, P. Lemmens, D. Wulferding, T. Shevtsova, A. Gusev, D. Chareev, and A. Vasiliev, *Phys. Rev. B* **87**, 144508 (2013).
- [62] P. B. Allen, *Phys. Rev. B* **6**, 2577 (1972).
- [63] P. Blaha, K. Schwarz, G. K. H. Madsen, D. Kvasnicka, and J. Luitz, *WIEN2K, An Augmented Plane Wave + Local Orbitals Program for Calculating Crystal Properties* (Karlheinz Schwarz, Techn. Universität Wien, Austria, 2001).
- [64] K. Haule, C.-H. Yee, and K. Kim, *Phys. Rev. B* **81**, 195107 (2010).
- [65] K. Haule and T. Birol, *Physical Review Letters* **115**, 256402 (2015).
- [66] K. Haule and G. L. Pascut, *Phys. Rev. B* **94**, 195146 (2016).
- [67] K. Haule, *Phys. Rev. B* **75**, 155113 (2007).
- [68] P. Werner, A. Comanac, L. de' Medici, M. Troyer, and A. J. Millis, *Physical Review Letters* **97**, 076405 (2006).
- [69] R. S. Kumar, Y. Zhang, S. Sinogeikin, Y. Xiao, S. Kumar, P. Chow, A. L. Cornelius, and C. Chen, *The Journal of Physical Chemistry B* **114**, 12597 (2010).
- [70] Y. Quan and Z. P. Yin, To be published.
- [71] Z. P. Yin, A. Kutevov, and G. Kotliar, *Phys. Rev. X* **3**, 021011 (2013).
- [72] Z. P. Yin, K. Haule, and G. Kotliar, *Nat Phys* **7**, 294 (2011).
- [73] Z. P. Yin, K. Haule, and G. Kotliar, *Nat Mater* **10**, 932 (2011).
- [74] A. Abrikosov, L. Gor'kov, and I. Dzyaloshinski, *Methods of Quantum Field Theory in Statistical Physics*, Dover Books on Physics Series (Dover Publications, 1975).
- [75] T. Shimojima, T. Sonobe, W. Malaeb, K. Shinada, A. Chainani, S. Shin, T. Yoshida, S. Ideta, A. Fujimori, H. Kumigashira, K. Ono, Y. Nakashima, H. An-

- zai, M. Arita, A. Ino, H. Namatame, M. Taniguchi, M. Nakajima, S. Uchida, Y. Tomioka, T. Ito, K. Kihou, C. H. Lee, A. Iyo, H. Eisaki, K. Ohgushi, S. Kasahara, T. Terashima, H. Ikeda, T. Shibauchi, Y. Matsuda, and K. Ishizaka, *Phys. Rev. B* **89**, 045101 (2014).
- [76] L. Fanfarillo, J. Mansart, P. Toulemonde, H. Cercellier, P. Le Fèvre, F. Bertran, B. Valenzuela, L. Benfatto, and V. Brouet, *Phys. Rev. B* **94**, 155138 (2016).
- [77] Y. S. Kushnirenko, A. A. Kordyuk, A. V. Fedorov, E. Haubold, T. Wolf, B. Büchner, and S. V. Borisenko, *Phys. Rev. B* **96**, 100504 (2017).
- [78] D. Guterding, H. O. Jeschke, and R. Valentí, *Phys. Rev. B* **96**, 125107 (2017).
- [79] L. Boeri, G. B. Bachelet, E. Cappelluti, and L. Pietronero, *Phys. Rev. B* **65**, 214501 (2002).
- [80] A. Goncharov and V. Struzhkin, *Physica C: Superconductivity* **385**, 117 (2003).